Ionics (2007) 13:195–203
DOI 10.1007/s11581-007-0097-8

ORIGINAL PAPER

Lithium ion conductivity of $Li_{5+x}Ba_xLa_{3-x}Ta_2O_{12}$ (x=0–2) with garnet-related structure in dependence of the barium content

Ramaswamy Murugan · Venkataraman Thangadurai · Werner Weppner

Received: 15 March 2007 / Accepted: 11 May 2007 / Published online: 19 June 2007

Abstract The stoichiometry range and lithium ion conductivity of $Li_{5+x}Ba_xLa_{3-x}Ta_2O_{12}$ (x=0, 0.25, 0.50, 1.00, 1.25, 1.50, 1.75, 2.00) with garnet-like structure were studied. The powder X-ray diffraction data of $Li_{5+x}Ba_xLa_{3-x}Ta_2O_{12}$ indicated that single phase oxides with garnet-like structure exist over the compositional range $0 \le x \le 1.25$; while for x= 1.5, 1.75 and 2.00, the presence of second phase in addition to the major garnet like phase was observed. The cubic lattice parameter increases with increasing x and reaches a maximum at x=1.25 then decreases slightly with further increase in x in $Li_{5+x}Ba_xLa_{3-x}Ta_2O_{12}$. The impedance plots of $Li_{5+x}Ba_xLa_{3-x}Ta_2O_{12}$ samples obtained at 33 °C indicated a minimum grain-boundary resistance (R_{gb}) contribution to the total resistance (R_b+R_{gb}) at x=1.0. The total (bulk+ grain boundary) ionic conductivity increases with increasing lithium and barium content and reaches a maximum at x= 1.25 and then decreases with further increase in x in $Li_{5+x}Ba_xLa_{3-x}Ta_2O_{12}$. Scanning electron microscope investigations revealed that $Li_{6.25}Ba_{1.25}La_{1.75}Ta_2O_{12}$ is much more dense, and the grains are more regular in shape. Among the investigated compounds, $Li_{6.25}Ba_{1.25}La_{1.75}Ta_2O_{12}$ exhibits the highest total (bulk+grain boundary) and bulk ionic conductivity of 5.0×10^{-5} and 7.4×10^{-5} S/cm at 33 °C, respectively.

Keywords Garnet-like structure · Solid electrolyte · Li ion conductivity · AC impedance · Fast ionic conduction

R. Murugan · W. Weppner (✉)
Sensors and Solid State Ionics, Faculty of Engineering,
University of Kiel,
Kaiserstr. 2.,
24143 Kiel, Germany
e-mail: ww@tf.uni-kiel.de

R. Murugan
e-mail: murugan@ac.uni-kiel.de

V. Thangadurai
Department of Chemistry, University of Calgary,
2500 University Drive NW,
Calgary, AB T2N 1N4, Canada
e-mail: vthangad@ucalgary.ca

Introduction

There is presently a strong ongoing search for materials for energy conversion and storage, e.g., both high- and low-temperature fuel cell electrolytes, high energy density rechargeable batteries, photo-electrochemical solar cells and hydrogen storage materials. Among the energy storage devices, rechargeable lithium ion batteries using lithium ion-conducting electrolytes have drawn much attention because of their wide range of use in portable electronic devices.

The presently commercially available lithium ion batteries use liquid organic electrolytes, which show major safety concern and short lifetime. These problems can be avoided by using solid lithium ion conducting electrolytes. Solid state lithium ion conductors (SSLICs) with the following properties:

(1) high ionic conductivity with negligible electronic conductivity
(2) long-term chemical stability with electrodes (both anode and cathode), especially in contact with metallic lithium or lithium alloy anodes
(3) high electrochemical stability (≥5.5 V/Li)

are expected to replace the presently used liquid electrolyte and allow the application of high-voltage cathode materials for improved energy density.

So far, all discovered inorganic electrolyte compounds had either high ionic conductivity or high electrochemical stability but not both [1–3]. In addition, some of the best lithium ion conductors, e.g., perovskite-type $Li_{3x}La_{(2/3)-x}\square_{(1/3)-2x}TiO_3$ ($0<x<0.16$; LLT), exhibit bulk conductivity of about 10^{-3} S/cm at 27 °C ($x\sim0.1$) and become predominantly electronic conductors within the lithium activity range given by the two electrodes [4–7]. As polycrystalline materials are being used for practical applications, large grain-boundary resistances are commonly observed in addition to the bulk resistance and therefore control the total (bulk+grain boundary) resistance of the galvanic cells. For instance, LLT exhibits a total (bulk+grain boundary) conductivity of 7×10^{-5} S/cm at 27 °C, which is about two orders of magnitude lower than that of the bulk ionic conductivity [4–7].

A novel class of fast lithium ion-conducting metal oxides with the nominal chemical composition $Li_5La_3M_2O_{12}$ (M=Nb, Ta) possessing garnet-related structure has been reported from our laboratory [8]. The bond valence analysis of Li^+-ion distribution confirms transport pathways, which relate to the experimentally observed high Li^+-ion conductivity [9]. The Li^+-ions move in a three-dimensional (3D) network of energetically equivalent partially occupied sites [9].

$Li_5La_3M_2O_{12}$ were only the first examples of fast lithium ion conductors possessing garnet-like structure and have prompted further investigations of conductivity optimization by chemical substitutions and structural modifications. Bond valence analysis of $Li_5La_3M_2O_{12}$ also predicted that the aliovalent substitutions at the La and M sites will significantly modify the connectivity of the network by controlling the number of easily accessible vacancies, and hence, the conductivity could be tailored further by appropriate chemical doping [9]. Accordingly, the partial substitution of divalent alkaline earth ions for a trivalent La in $Li_5La_3M_2O_{12}$ yielded a novel series of garnet-like structure compounds with the general chemical formula of $Li_6ALa_2Nb_2O_{12}$ (A=Ca, Sr, Ba) [10] and $Li_6ALa_2Ta_2O_{12}$ (A=Sr, Ba) [11, 12]. Partial substitution of trivalent La by monovalent K and pentavalent Nb by trivalent In in $Li_5La_3Nb_2O_{12}$ yielded also new members of SSLICs with garnet-like structure [13]. Recent neutron diffraction studies on the structure of $Li_5La_3M_2O_{12}$ revealed that Li^+ is located on both tetrahedral and octahedral sites, and the latter ones are responsible for the observed high Li^+ mobility through a clustering mechanism [14]. Structure- and ionic-transport properties of $Li_3Ln_3Te_2O_{12}$ (Ln=Y, Pr, Nd, Sm-Lu) reported by O'Callaghan et al. [15] revealed that Li^+ will preferentially occupy the tetrahedral site in this series, and $Li_3Nd_3Te_2O_{12}$ exhibited the maximum observed conductivity of 10^{-5} S/cm at 600 °C with an activation energy of 1.2 eV.

The earlier studies clearly indicated the ability of the garnet-like structure $Li_5La_3M_2O_{12}$ to accommodate varying sizes of divalent alkaline earth ions for trivalent La with no change in symmetry [10, 11]. Moreover, the substitution of the bigger cations Sr^{2+} and Ba^{2+} for smaller La^{3+} in $Li_5La_3Ta_2O_{12}$ increases the lattice parameter as well as the ionic conductivity [11]. Among the investigated compounds with garnet-related structure, $Li_6BaLa_2Ta_2O_{12}$ exhibited the highest Li^+-ion conductivity of 4×10^{-5} Scm^{-1} at 22 °C with an activation energy of 0.4 eV [11], and this material has overcome the existing problems of electrolytes, i.e., lack of high ionic conductivity with good chemical and electrochemical stability, and very low grain-boundary resistance at room temperature for battery application [11, 12].

In the present work, we report systematic studies on structure and transport properties by the simultaneous substitution of lanthanum by barium and lithium according to the formula $Li_{5+x}Ba_xLa_{3-x}Ta_2O_{12}$ (x=0, 0.25, 0.50, 1.00, 1.25, 1.50, 1.75, 2.00) for further understanding of the stoichiometric range and ionic conductivity dependence on both the crystal lattice parameter and the carrier concentration.

Experimental

Materials preparation and phase characterisation

Conventional solid state reaction procedure was employed to prepare the title compounds. Required amounts of high purity chemicals $LiNO_3$ (Sigma-Aldrich, >99%; 10 wt% excess was added to compensate for the loss of lithium during annealing), $Ba(NO_3)_2$ (Riedel-deHaen, >99%), La_2O_3 (Alfa Aesar, >99.9%; pre-dried at 900 °C for 24 h) and Ta_2O_5 (Alfa Aesar, >99.85%) were ball-milled using zirconia balls in 2-propanol for about 12 h. After the evaporation of solvents at room temperature, the mixtures were heated in air from room temperature to 700 °C at a rate of 2 °C min^{-1} in an open alumina crucible and held at this temperature for 12 h and then cooled down to room temperature. The resultant powders were ground again for another 12 h using zirconia balls in 2-propanol. After the evaporation of solvents, the powders were pressed into pellets by isostatic pressure. The pellets were covered with the same mother powder to reduce possible lithium loss and heated in air from room temperature to 900 °C at a rate of 2.5 °C min^{-1} and held at this temperature for 24 h. The sintered pellets were cut into small pellets using a diamond saw. Powder X-ray diffraction (XRD; SEIFERT 3000, CuK_α, Germany) was employed to monitor the phase formation. The lattice constant was determined from powder XRD data by least-squares refinement. A scanning electron microscope (SEM; PHILIPS XL 30 Series, The Netherlands) was used to monitor the surface morphology of the sample pellets.

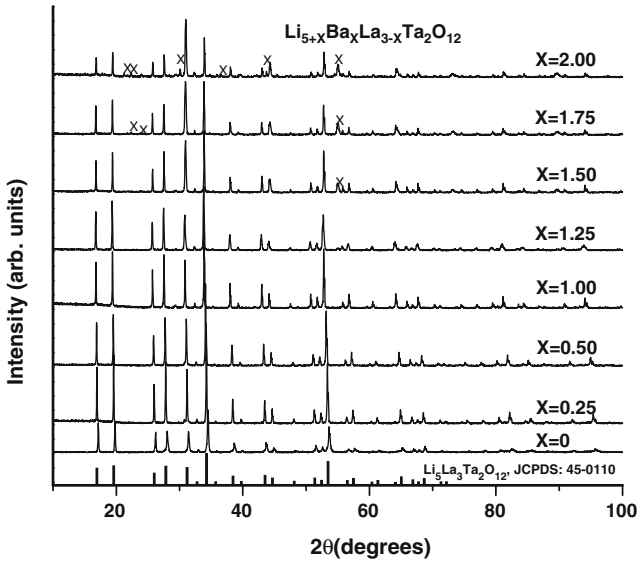

Fig. 1 Powder XRD patterns of $Li_{5+x}Ba_xLa_{3-x}Ta_2O_{12}$ (x=0, 0.25, 0.50, 1.00, 1.25, 1.50, 1.75, 2.00) together with the standard pattern of $Li_5La_3Ta_2O_{12}$ reported by Joint Committee on Powder Diffraction Standards (*JCPDS*: 45-0110). *X* indicates unknown second phase contribution

Electrical characterisation

Electrical conductivity measurements of the pellets (0.16–0.18 cm in thickness and 0.90–1.1 cm in diameter) were performed in argon using Li-ion-blocking Au-electrodes (Au paste cured at 700 °C for 1 h) in the temperature range from 17 to 350 °C using an Impedance and Gain-Phase Analyzer (HP 4192 A, Hewlett-Packard Co., Palo Alto, CA; 5 Hz−13 MHz). Before each impedance measurement, the samples were equilibrated for 3–6 h at constant temperature. For each sample, the impedance measurements were made for both heating and cooling cycle.

Results

Powder XRD

Figure 1 shows the variation in the measured powder XRD patterns for the compositions $Li_{5+x}Ba_xLa_{3-x}Ta_2O_{12}$ (x=0, 0.25, 0.50, 1.00, 1.25, 1.50, 1.75, 2.00) together with the standard pattern of $Li_5La_3Ta_2O_{12}$ reported in the Joint Committee on Powder Diffraction Standards (JCPDS: 45-0110). The powder XRD patterns shown in Fig. 1 indicate that a garnet-like solid solution with a similar pattern is formed in the range up to x=1.25. The measured powder XRD patterns for x=1.5, 1.75 and 2.00 indicate the presence of a second phase in addition to the major garnet-related phase.

Electrical properties

AC impedance

Typical impedance plots of $Li_{5+x}Ba_xLa_{3-x}Ta_2O_{12}$ with x= 0, 0.25, 0.50, 1.00 and x=1.25, 1.50, 1.75 measured at 33 and 50 °C, respectively, are shown in Figs. 2 and 3. The impedance plots could be resolved into bulk, grain-boundary and electrode contributions. The composition dependence of the bulk, grain-boundary and total (bulk+

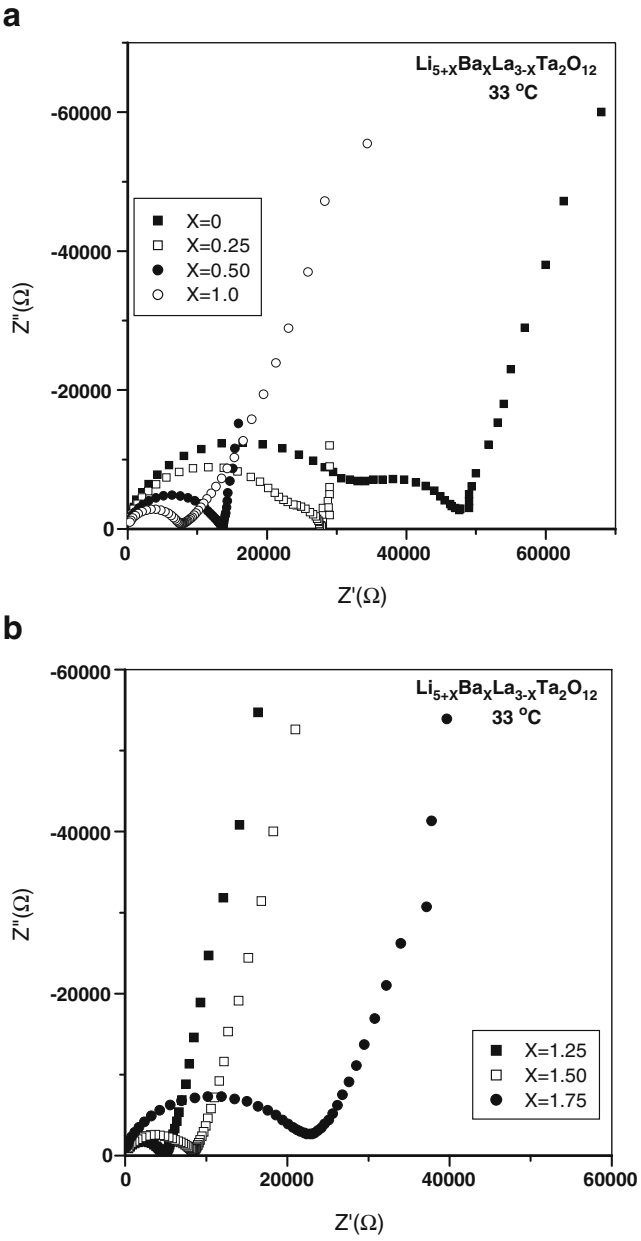

Fig. 2 AC impedance plots of $Li_{5+x}Ba_xLa_{3-x}Ta_2O_{12}$ **a** at x=0, 0.25, 0.50, 1.00 and **b** at x=1.25, 1.50, 1.75 measured in slowly flowing argon at 33 °C using lithium ion-blocking Au electrodes

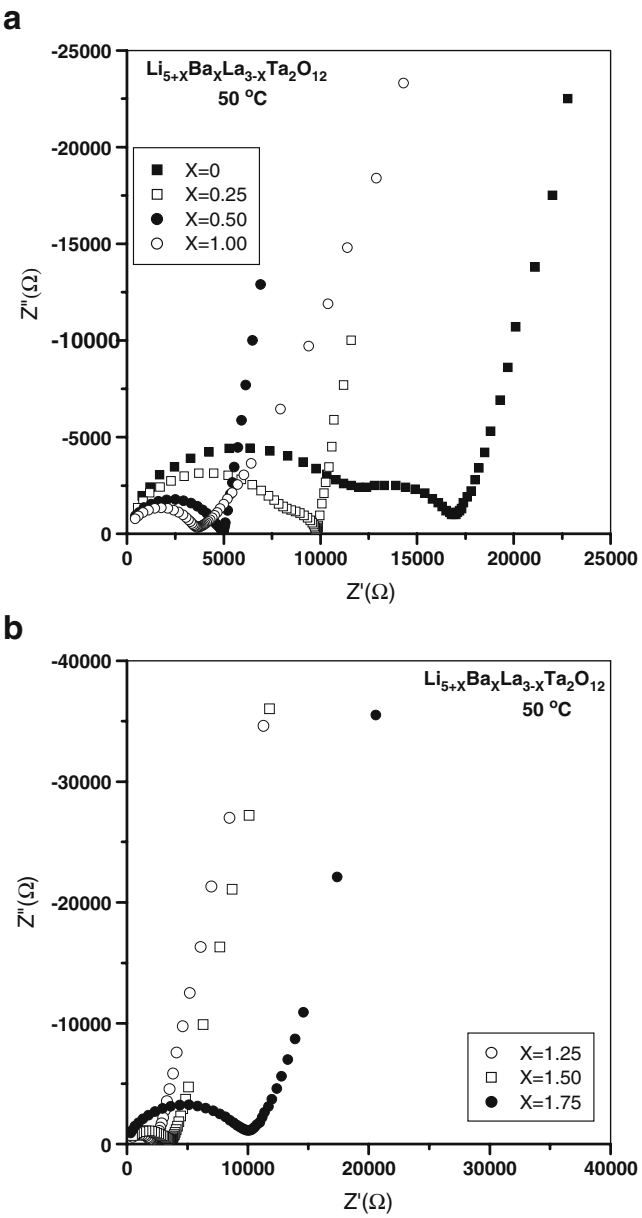

Fig. 3 AC impedance plots of $Li_{5+x}Ba_xLa_{3-x}Ta_2O_{12}$ **a** at x=0, 0.25, 0.50, 1.00 and **b** at x=1.25, 1.50, 1.75 measured in slowly flowing argon at 50 °C using lithium ion blocking Au electrodes

grain boundary) resistance of $Li_{5+x}Ba_xLa_{3-x}Ta_2O_{12}$ samples derived from the impedance measurements at 33 °C are presented in Fig. 4. To understand the grain-boundary resistance contribution to the total (bulk+grain boundary) resistance of the $Li_{5+x}Ba_xLa_{3-x}Ta_2O_{12}$ samples, the data derived from the impedance measurements at 33 °C are plotted in Fig. 5 as $R_{gb}/(R_b+R_{gb})$ and total resistance (R_b+R_{gb}) versus x in $Li_{5+x}Ba_xLa_{3-x}Ta_2O_{12}$. At higher temperature (>50 °C), it is difficult to separate bulk and grain-boundary contribution accurately. For experimental and practical reasons of applications, we have considered uniformly the total (bulk+grain boundary) contribution for the presentation

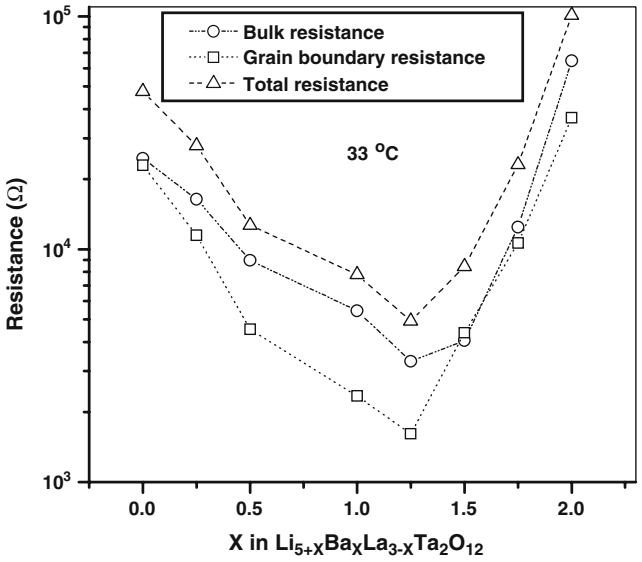

Fig. 4 Bulk, grain-boundary and total (bulk+grain boundary) resistance derived from the impedance plots of $Li_{5+x}Ba_xLa_{3-x}Ta_2O_{12}$ samples measured at 33 °C

of the electrical conductivity over the investigated temperature range.

Total (bulk+ grain boundary) electrical conductivity

Arrhenius plots for the total (bulk+grain boundary) electrical conductivity of $Li_{5+x}Ba_xLa_{3-x}Ta_2O_{12}$ with x=0, 0.25, 0.50, 1.00 and x=1.25, 1.50, 1.75, 2.00 are shown in Figs. 6a and b, respectively. The data obtained from heating and cooling cycles follow the same line, suggesting that the measured values are equilibrium data. For comparison, the Arrhenius plots for the total (bulk+grain boundary)

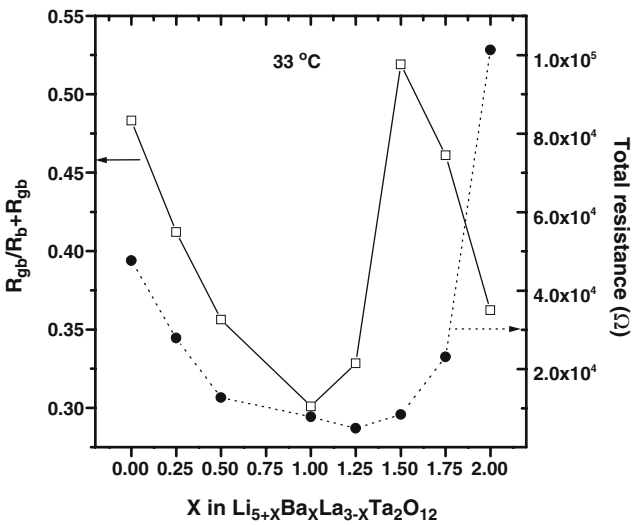

Fig. 5 Ratio of grain-boundary resistance (R_{gb}) and total resistance (R_b+R_{gb}) and total resistance (R_b+R_{gb}) versus x in $Li_{5+x}Ba_xLa_{3-x}Ta_2O_{12}$ derived from the impedance plots measured at 33 °C

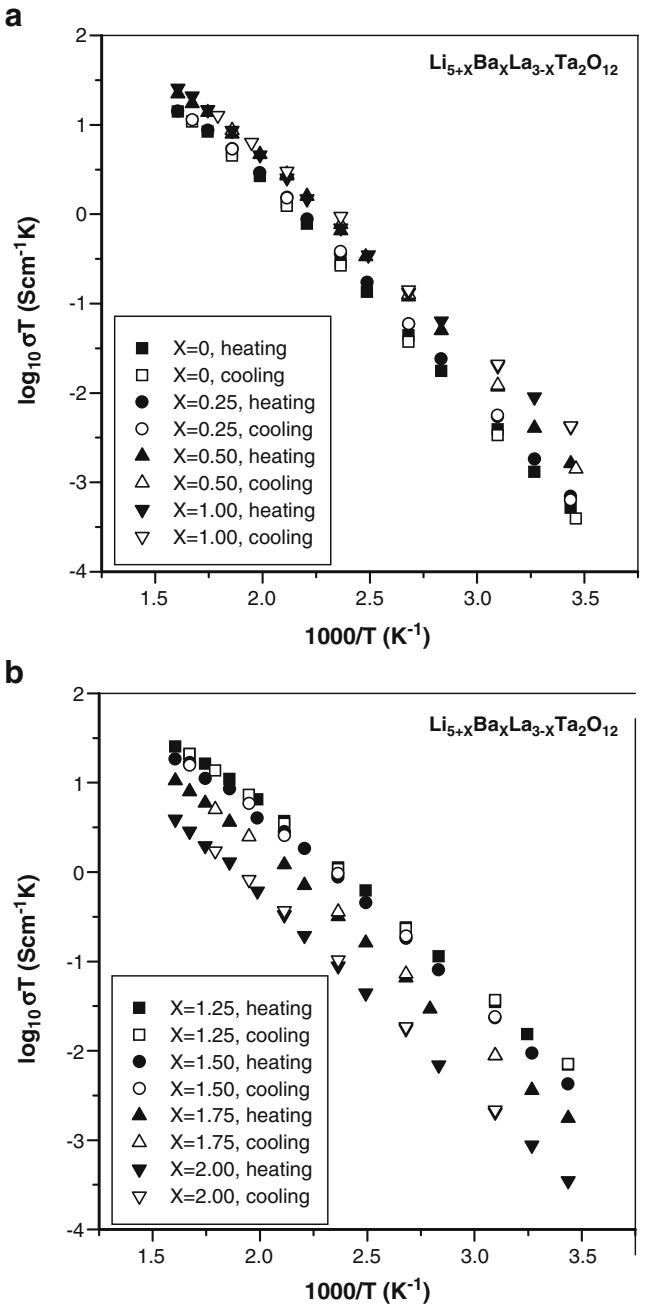

Fig. 6 Arrhenius plots for the total (bulk+grain boundary) lithium ion conductivity of $Li_{5+x}Ba_xLa_{3-x}Ta_2O_{12}$ **a** at x=0, 0.25, 0.50, 1.00 and **b** at x=1.25, 1.50, 1.75, 2.0. The data were obtained for a heating and cooling cycle and followed the same line

electrical conductivity of $Li_{5+x}Ba_xLa_{3-x}Ta_2O_{12}$ with x=0, 0.25, 0.50, 1.00, 1.25, 1.50, 1.75, 2.00 measured during heating are shown in Fig. 7. The activation energies (E_a) for the ionic conductivity (σ) were determined from the Arrhenius plots employing the equation:

$$\sigma T = A \exp\left[\frac{-Ea}{kT}\right], \quad (1)$$

where A, T and k are the pre-exponential parameter, absolute temperature and Boltzmann's constant, respectively.

The composition dependence of the total (bulk+grain boundary) electrical conductivity of $Li_{5+x}Ba_xLa_{3-x}Ta_2O_{12}$ is shown in Fig. 8 at various temperatures. From this figure, it is observed that at each temperature, the total (bulk+grain boundary) conductivity increases with increasing x and reaches a maximum at x=1.25 then decreases with further increase in x in $Li_{5+x}Ba_xLa_{3-x}Ta_2O_{12}$.

Discussion

Structural description

The powder XRD patterns (Fig. 1) of the investigated compounds in the series $Li_{5+x}Ba_xLa_{3-x}Ta_2O_{12}$ (x up to 1.25) indicate garnet-like solid solutions with a similar pattern to that of the parent compound $Li_5La_3Ta_2O_{12}$ [8, 9]. However, further increase in x (x>1.25) leads to the presence of a second phase in addition to the major garnet-like phase. The lattice parameter determined from powder XRD data by least-squares refinement revealed an increase in the cubic lattice constant with the increase in x in $Li_{5+x}Ba_xLa_{3-x}Ta_2O_{12}$ and reaches a maximum of 12.993(4) Å corresponding to $Li_{6.25}Ba_{1.25}La_{1.75}Ta_2O_{12}$ and then decreases with further increase in x in $Li_{5+x}Ba_xLa_{3-x}Ta_2O_{12}$.

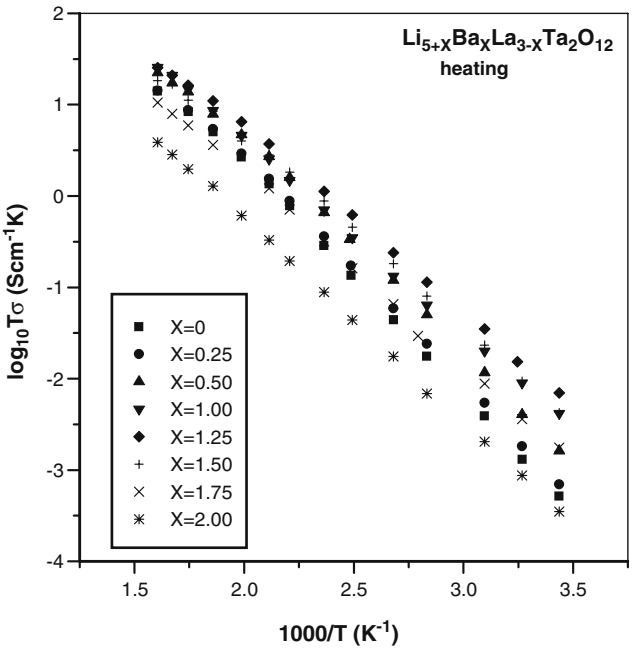

Fig. 7 Comparison of the Arrhenius plots for the total (bulk+grain boundary) lithium ion conductivity of $Li_{5+x}Ba_xLa_{3-x}Ta_2O_{12}$ at x=0, 0.25, 0.50, 1.00, 1.25, 1.50, 1.75, 2.0 during heating

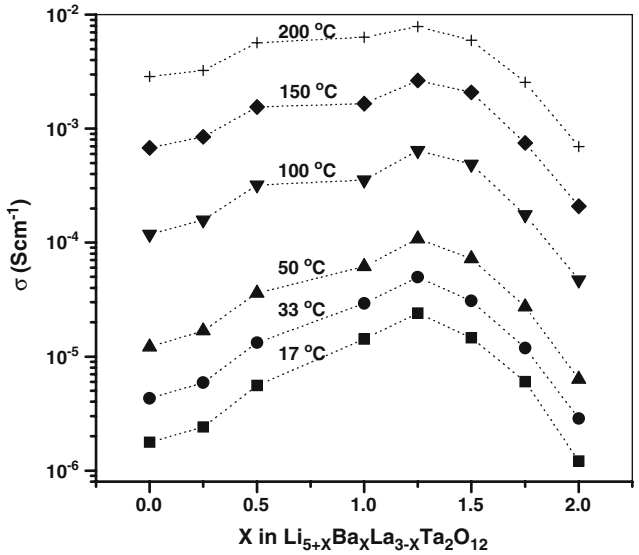

Fig. 8 Composition dependencies of the total (bulk+grain boundary) conductivity of $Li_{5+x}Ba_xLa_{3-x}Ta_2O_{12}$ samples at various temperatures

Garnets are orthosilicates with the general formula $A_3^{II}B_2^{III}(SiO_4)_3$ (A=Ca, Mg, Y or Ln=La or rare earth elements; B=Al, Fe, Ga, Ge, Mn, Ni, V), and A and B occupy eight and six coordinated cation sites [16], respectively. The structure of $Li_5La_3M_2O_{12}$ (M=Nb, Ta) has been determined in 1988 from powder XRD data by Mazza [17] as well as from single-crystal data by Hyooma and Hayashi [18]. Mazza [17] described the structure as being closely related to the garnet structure (SG $Ia\bar{3}d$ [no. 230], a=12.8 Å, La^{3+} on the A^{II} site $^1/_8$, 0, $^1/_4$; Nb^{5+} or Ta^{5+} on the B^{III} site 0, 0, 0; three of the Li^+ on the tetrahedrally coordinated Si^{IV} site $^3/_8$, 0, $^1/_4$) with the exception that two additional Li^+ per formula unit should fully occupy the octahedrally coordinated site $^1/_8$, $^1/_8$, $^1/_8$ that is vacant in the ideal garnet structure. In this structure model, only the oxygen site contains refinable atomic coordinates (three refinable atomic coordinates). Hyooma and Hayashi [18], however, proposed a lower symmetry non-centrosymmetric space group $I2_13$ (no. 199). Bond valence mismatch calculation has been carried out to control the chemical plausibility of the published structure models and to identify probable pathways for Li^+ ionic motion in $Li_5La_3M_2O_{12}$ (M=Nb, Ta) [9]. Recently, neutron diffraction studies by Cussen [14] revealed that $Li_5La_3M_2O_{12}$ crystallises in the space group $Ia\bar{3}d$, and Li^+ is located on both tetrahedral and octahedral sites and that clusters of mobile Li^+ exist within these materials. We believe that lithium ions in the investigated materials occupy both the tetrahedral and octahedral sites. Neutron diffraction study is required to determine the structure of the presently investigated garnets.

Electrical properties

AC impedance

The appearance of a low-frequency tail (Figs. 2 and 3) in case of ionically blocking electrodes is an indication that the conductivity of the investigated garnet-type compounds is ionic in nature [19–21]. The impedance plots of $Li_{5+x}Ba_xLa_{3-x}Ta_2O_{12}$ measured at low temperature (Figs. 2 and 3) could be resolved into bulk, grain-boundary and electrode resistances corresponding to an equivalent circuit consisting of a series of two parallel resistance-capacitance and capacitance contributions [19–21]. A similar behaviour has been observed for the earlier investigated garnet-related structure materials [8, 10, 11, 13]. The impedance plots of $Li_{5+x}Ba_xLa_{3-x}Ta_2O_{12}$ samples measured at higher temperature exhibit nearly a single semicircle for the bulk conductivity contribution at high frequencies and a tail in the low frequency regime for blocking electrodes for the mobile lithium ions.

The bulk, grain-boundary and total (bulk+grain boundary) resistance of $Li_{5+x}Ba_xLa_{3-x}Ta_2O_{12}$ samples derived from the impedance measurements at 33 °C as presented in Fig. 4 indicate an appreciable decrease in the bulk, grain-boundary and total (bulk+grain boundary) resistance values with increasing x, reaching a minimum at x=1.25. With further increase in x (x>1.25), the bulk, grain-boundary and total (bulk+grain boundary) resistance increase. The data plotted as $R_{gb}/(R_b+R_{gb})$ and (R_b+R_{gb}; total resistance) versus x in $Li_{5+x}Ba_xLa_{3-x}Ta_2O_{12}$ in Fig. 5 indicate that the grain-boundary resistance contribution to the total (bulk+grain boundary) resistance initially decreases with increasing of x and reaching a minimum contribution for x=1 in Li_{5+x} $Ba_xLa_{3-x}Ta_2O_{12}$. However, with further increase in x

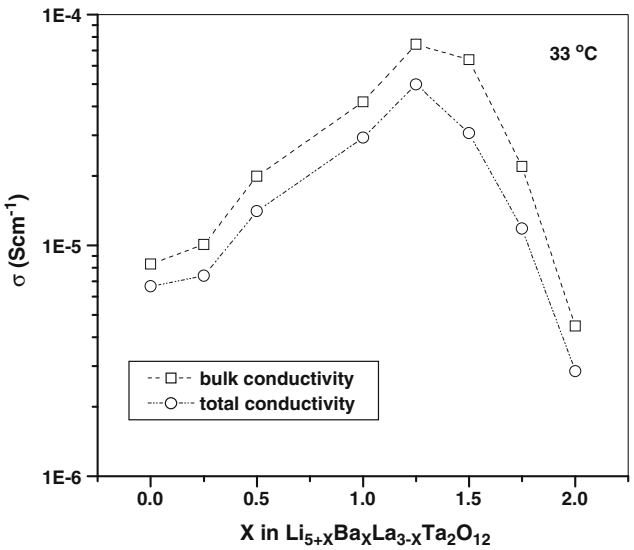

Fig. 9 Composition dependencies of the bulk and total (bulk+grain boundary) conductivity of $Li_{5+x}Ba_xLa_{3-x}Ta_2O_{12}$ samples at 33 °C

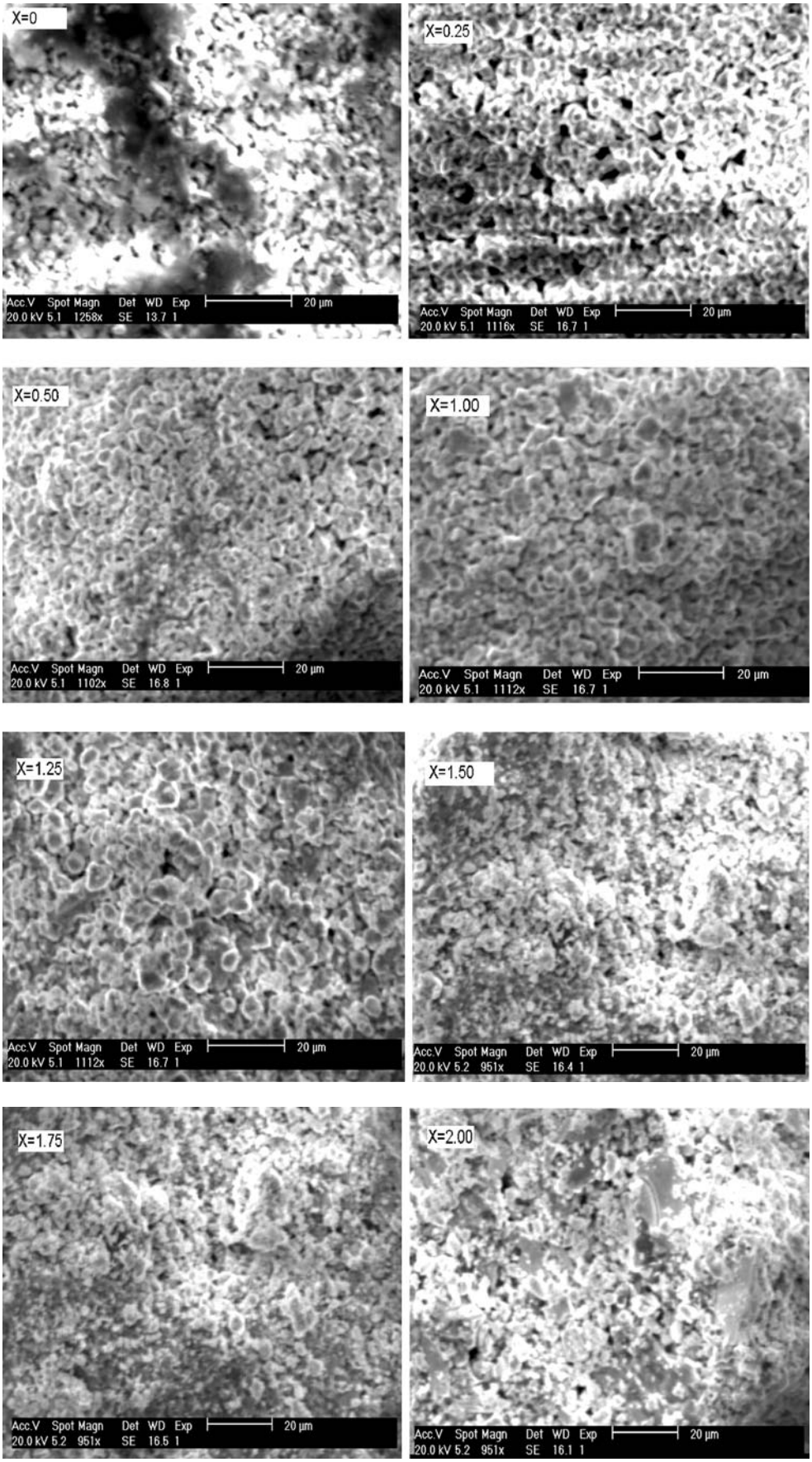

Fig. 10 SEM images of $Li_{5+x}Ba_xLa_{3-x}Ta_2O_{12}$ at x=0, 0.25, 0.50, 1.00, 1.25, 1.50, 1.75 and 2.0

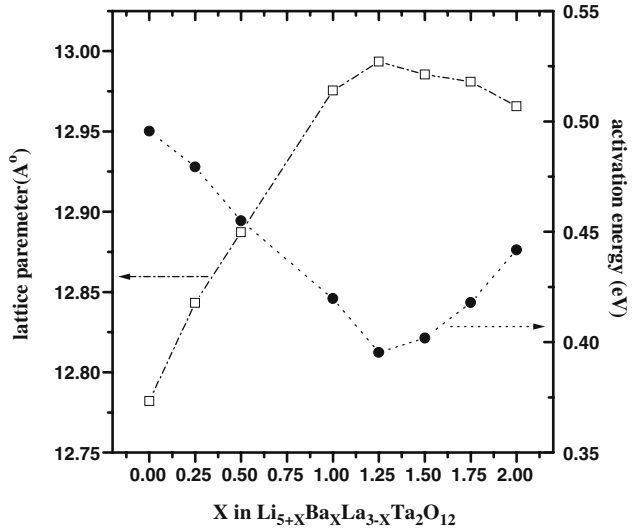

Fig. 11 Composition dependencies of the lattice parameter and activation energy of $Li_{5+x}Ba_xLa_{3-x}Ta_2O_{12}$

(x=1.25 and 1.5), $Li_{5+x}Ba_xLa_{3-x}Ta_2O_{12}$ exhibits an increase in the contribution of the grain-boundary resistance to the total (bulk+grain boundary) resistance. With further increase in x (x=1.75 and 2), there is again a decrease in the grain-boundary resistance contribution to the total (bulk+grain boundary) resistance.

The Arrhenius plots for the total (bulk+grain boundary) electrical conductivity of $Li_{5+x}Ba_xLa_{3-x}Ta_2O_{12}$ with x=0, 0.25, 0.50, 1.00 and x=1.25, 1.50, 1.75, 2.00 shown in Figs. 6a and b, respectively, indicate that there is no major shift in the conductivity for the heating and cooling cycles. This implies that the investigated compounds with garnet-like structure are stable without any phase transition in the investigated temperature range. In Fig. 7, we compare the Arrhenius plots for the total (bulk+grain boundary) electrical conductivity of $Li_{5+x}Ba_xLa_{3-x}Ta_2O_{12}$ (with x=0, 0.25, 0.50, 1.00, 1.25, 1.50, 1.75, 2.00) during heating. As expected, among the investigated samples, the composition $Li_{5+x}Ba_xLa_{3-x}Ta_2O_{12}$ with x=1.25 exhibits the highest conductivity with the lowest activation energy of 0.4 eV.

The composition dependence of the total (bulk+grain boundary) electrical conductivity of $Li_{5+x}Ba_xLa_{3-x}Ta_2O_{12}$ at various temperatures shown in Fig. 8 clearly reveals that the total (bulk+grain boundary) conductivity increases with increasing x and reaches a maximum at x=1.25 then decreases with further increase in x in $Li_{5+x}Ba_xLa_{3-x}Ta_2O_{12}$. Among the investigated compounds, $Li_{6.25}Ba_{1.25}La_{1.75}Ta_2O_{12}$ exhibits the highest total (bulk+grain boundary) ionic conductivity of 2.4×10^{-5} S/cm at 17 °C with an activation energy of 0.4 eV. The decrease in the total (bulk+grain boundary) electrical conductivity of $Li_{5+x}Ba_xLa_{3-x}Ta_2O_{12}$ with x>1.25 may be due to the formation of second phase in the grain-boundary region. Figure 9 depicts the composition dependencies of bulk and total (bulk+grain boundary) conductivity of $Li_{5+x}Ba_xLa_{3-x}Ta_2O_{12}$ samples at 33 °C. Similar to the total (bulk+grain boundary) conductivity, the bulk conductivity also increases with increase in x and reaches maximum at x=1.25 with a total (bulk+grain boundary) conductivity of 5×10^{-5} S/cm and a bulk conductivity of 7.4×10^{-5} S/cm and then decreases with further increase in x in $Li_{5+x}Ba_xLa_{3-x}Ta_2O_{12}$.

Preliminary work on the influence of the microstructure on the ionic conductivity of $Li_{5+x}Ba_xLa_{3-x}Ta_2O_{12}$ (x=0, 0.25, 0.50, 1.00, 1.25, 1.50, 1.75, 2.00) prepared under the same sintering conditions was carried out. SEM images shown in Fig. 10 indicate increasing grain size and regular shape with increasing x and provides larger grain size at x=1.25 and thereafter with further increase in x, a non-uniform microstructure because of agglomeration. The large grain size and more regular shape observed at x=1.0 and 1.25 is due to the simultaneous addition of lithium and barium content. Particularly, lithium addition acts as flux to increase the sinterability of the ceramic oxides. Accordingly, these compounds are much more dense, posses better crystallinity and more regular grain shape, which results in the high conductivity with low activation energy observed in these samples compared to that of other compounds. However, further increase in lithium and barium content (x=1.5, 1.75 and 2) leads to non-uniform microstructure because of the agglomeration and the appearance of the second phase together with the major garnet phase and consequently causes a reduction in the conductivity with high activation energy in these compounds.

The variation of the activation energy and lattice parameter with x in $Li_{5+x}Ba_xLa_{3-x}Ta_2O_{12}$, as shown in Fig. 11, clearly indicates an increase in the cubic lattice parameter with increasing x and reaches a maximum for x= 1.25 and then decreases slightly with further increase in x. As expected, the activation energy decreases with increasing x in $Li_{5+x}Ba_xLa_{3-x}Ta_2O_{12}$ then reaches a minimum at x= 1.25 and increases again with further increase in x. The increase in conductivity with decreasing activation energy accompanied by the lattice expansion for the investigated samples in this $Li_{5+x}Ba_xLa_{3-x}Ta_2O_{12}$ series ($0\le x\le1.25$) indicates that there is a systematic correlation between the lattice expansion by alkaline earth divalent Ba substitution and simultaneous increase in lithium ion concentration with the increase in ionic conductivity.

Summary

Formation of solid solutions with garnet-like structure and ionic conductivity were investigated for the series $Li_{5+x}Ba_xLa_{3-x}Ta_2O_{12}$. The powder XRD data of $Li_{5+x}Ba_xLa_{3-x}$

Ta_2O_{12} indicate that single phase oxides with garnet-like structure are formed over the composition range $0 \leq x \leq 1.25$. The samples became mixtures of the solid solution and an unknown second phase beyond the solid-solution limit. A minimum contribution of the grain-boundary resistance to the total (bulk+grain boundary) resistance was observed for $x=1$ in $Li_{5+x}Ba_xLa_{3-x}Ta_2O_{12}$. The total (bulk+grain boundary) and bulk ionic conductivity increase with increasing lithium and barium content and reach a maximum corresponding to $x=1.25$ then decrease with further increase in x in $Li_{5+x}Ba_xLa_{3-x}Ta_2O_{12}$. As expected, the activation energy for $x=1.25$ in $Li_{5+x}Ba_xLa_{3-x}Ta_2O_{12}$ shows a minimum and interestingly for this composition, the lattice parameter is found to show a maximum in this solid solution. Among the investigated compounds, $Li_{6.25}Ba_{1.25}La_{1.75}Ta_2O_{12}$ exhibits the highest total (bulk+grain boundary) and bulk ionic conductivity of 5×10^{-5} and 7.4×10^{-5} S/cm at 33 °C, respectively.

Acknowledgements Authors would like to thank the German Science Foundation (DFG, grant WE 684/11-1) for financial support.

Note: Independent of our studies, M.P. O'Callaghan and E.J. Cussen (Chem. Commun., 2007, 2048) have recently reported structural investigations on the same series of compositions.

References

1. Robertson AD, West AR, Ritchie AG (1997) Solid State Ionics 104:1
2. Aono H, Imanaka H, Adachi GY (1994) Acc Chem Res 27:265
3. Adachi GY, Imanaka N, Aono H (1996) Adv Mater 8:127
4. Inaguma Y, Liquan C, Itoh M, Nakamura T, Uchida T, Ikuta H, Wakihara W (1993) Solid State Commun 86:689
5. Birke P, Scharner S, Huggins RA, Weppner W (1997) J Electrochem Soc 144:L167
6. Kawai H, Kuwano J (1994) J Electrochem Soc 141:L78
7. Stramare S, Thangadurai V, Weppner W (2003) Chem Mater 15:3974
8. Thangadurai V, Kaack H, Weppner W (2003) J Am Ceram Soc 86:437
9. Thangadurai V, Adams S, Weppner W (2004) Chem Mater 16:2998
10. Thangadurai V, Weppner W (2005) J Am Ceram Soc 88:411
11. Thangadurai V, Weppner W (2005) Adv Funct Mater 15:107
12. Thangadurai V, Weppner W (2005) J Power Sources 142:339
13. Thangadurai V, Weppner W (2006) J Solid State Chem 179:974
14. Cussen E J (2006) Chem Commun 412
15. O'Callaghan MP, Lynham DR, Cussen EJ, Chen GZ (2006) Chem Mater 18:4681
16. Wells AF (1984) Structural inorganic chemistry, 5th edn. Clarendon, Oxford
17. Mazza D (1988) Mater Lett 7:205
18. Hyooma H, Hayashi K (1988) Mater Res Bull 23:1399
19. Thangadurai V, Huggins RA, Weppner W (2002) J Power Sources 108:64
20. Irvine JTS, Sinclair DC, West AR (1990) Adv Mater 2:132
21. Bauerle JE (1969) J Phys Chem Solids 30:2657